ANALYZING TOMOGRAPHIC SAR DATA OF A FOREST WITH RESPECT TO FREQUENCY, POLARIZATION AND FOCUSING TECHNIQUE

Othmar Frey and Erich Meier

Remote Sensing Laboratories
University of Zurich, Switzerland

ABSTRACT

Forest canopies are semi-transparent to microwaves at both, L- and P-Band. Thus, potentially, a number of scattering sources and different types of scattering mechanisms may contribute to a single range cell of a SAR image. By appropriately combining SAR data of multiple parallel flight paths a large two-dimensional aperture is synthesized which allows for tomographic imaging of the three-dimensional structure of such semi-transparent media.

Using a time-domain back-projection based focusing algorithm in combination with three tomographic focusing techniques (multi-look standard beamforming, robust Capon beamforming, and MUSIC) a 3D volume containing a forested area has been tomographically imaged at L- and P-band.

In this paper, an analysis of the two fully-polarimetric tomographic SAR data sets with respect to the localization of scattering sources and scattering mechanisms is given. In particular, the 3D data is examined regarding the performance of the three different tomographic focusing techniques, as well as for both, the two frequency bands and the different polarimetric channels.

Index Terms— SAR Tomography, Multibaseline SAR, Beamforming, Capon, MUSIC, E-SAR, L-Band, P-Band

1. INTRODUCTION

Research towards improving the knowledge about the backscattering behavior of forests with the goal of estimating biophysical parameters by means of synthetic aperture radar (SAR) tomography has become a major topic within the SAR remote sensing community [1–3]. With prospective spaceborne SAR remote sensing missions BIOMASS and Tandem-L at P-band and L-band these frequency bands have even gained in importance.

In September 2006, an airborne SAR campaign has been flown by the German Aerospace Center's E-SAR system over a test site in Switzerland [4], where two fully polarimetric tomographic data sets (P-band and L-band) of a partially forested area have been taken (see Table 1 for the sensor specifications and a summary of the parameters which characterize the tomographic data sets).

	P-band	**L-band**
Carrier frequency	350 MHz	1.3 GHz
Chirp bandwidth	70 MHz	94 MHz
Sampling rate	100 MHz	100 MHz
PRF	500 Hz	400 Hz
Ground speed	90 m/s	90 m/s
No. of data tracks	11+1	16+1
Nominal track spacing d_n	57 m	14 m
Horizontal baselines	40 m	10 m
Vertical baselines	40 m	10 m
Synthetic aperture in normal direction L	570 m	210 m
Nominal resolution in normal direction δ_n	3 m	2 m
Approx. unambiguous height H	30 m	30 m

Table 1. E-SAR system specifications and nominal parameters of the tomographic acquisition patterns.

Meanwhile, an analysis of the localization of the main back-scattering elements obtained by means of tomographic processing of the two (L- and P-band) airborne fully-polarimetric multibaseline SAR data sets of a forested area using three different focusing techniques (MLBF, Capon, MUSIC) has been carried out.

In this paper, the processing approach is sketched and excerpts from the data analysis are presented.

In particular, we have (1) included a full three-dimensional image of the forest obtained from the L-band tomographic data set and having applied the Multiple Signal Classification method (see Fig. 1) for focusing in the normal direction; (2) vertical slices through the volume are presented for the L-band case and all focusing methods employed (MLBF, Capon, and MUSIC) (see Fig. 2); (3) the tomographic focusing performance is shown for both wavelengths and the three focusing methods, respectively, (see Fig. 3) and (4) vertical profiles of the back-scattering amplitude for both the P-band and the L-band data set are given (see Fig. 4).

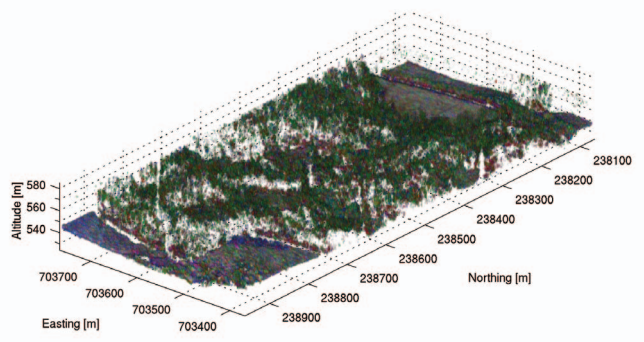

Fig. 1. Tomographic image (3D voxel plot) of a partially forested area obtained from combined TDBP and MUSIC beamforming of polarimetric airborne repeat-pass multibaseline SAR data at L-band. For better visual appearance each channel has been scaled individually. Red (HH), green (HV), blue (VV). Low intensity = high transparency of the voxel.

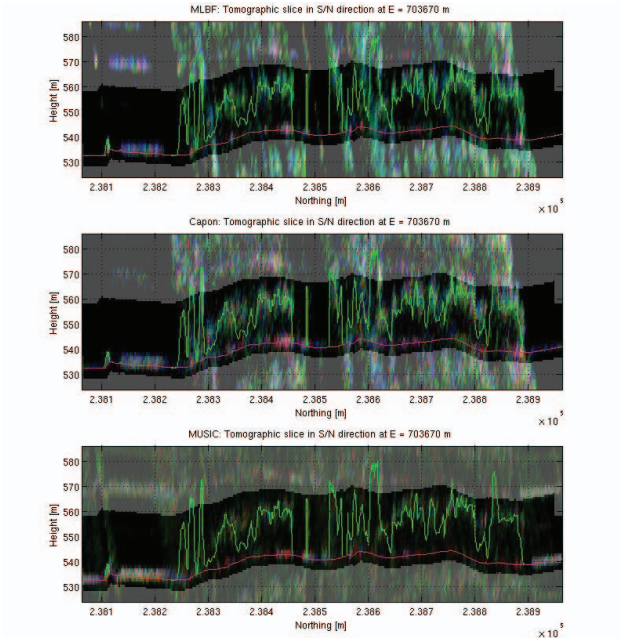

Fig. 2. Vertical slice through 3D volume of a forested area obtained from the polarimetric multibaseline L-Band data set using all (16) data tracks. Red (HH), green (HV), blue (VV). Top: Multi-look beamforming, middle: robust Capon beamforming, bottom: MUSIC. Greyed area indicates ambiguous target region.

2. TOMOGRAPHIC FOCUSING

2.1. Multi-Look Standard Beamforming

The standard multi-look beamforming approach has been applied using the time-domain back-projection based approach described in [5].

2.2. Multiple Signal Classification

In the following the main steps to compute the location of the scatterers based on MUSIC [6] is given:

1. Calculate the sample covariance matrix $\mathbf{R}$.

2. Calculate the eigen-decomposition of the sample covariance matrix

$$\mathbf{R} = \mathbf{U}\mathbf{D}\mathbf{U}^H \tag{1}$$

3. Permute the elements of the matrices such that the eigenvalues in $\mathbf{D}$ are sorted in nonincreasing order: $\gamma_1 \geq \gamma_2 \geq ... \geq \gamma_K$; the matrix of eigenvectors $\mathbf{U}$ is adjusted accordingly.

4. Set a threshold for the eigenvalue that separates the signal- and the noise-subspace, respectively.

5. Estimate the locations of the sources by evaluating

$$\hat{P}_M = \frac{1}{\mathbf{a}^H \mathbf{G}\mathbf{G}^H \mathbf{a}} \tag{2}$$

where $G = [\mathbf{u}_{p+1}...\mathbf{u}_K]$ contains the eigenvectors that span the noise space, and $\mathbf{a}$ is the steering vector.

2.3. Robust Capon Beamforming

While the MUSIC algorithm possesses an inherent robustness against steering vector errors, as has been shown in [7], in the case of the Capon beamformer, an improved resolution and a better reduction of the sidelobes can either be obtained if the steering vector is calibrated perfectly, or, if the Capon beamformer is extended in such a way that the unknown true steering vector $\mathbf{a}$ is estimated along with the power P_C.

Li et al. [8] and Stoica et al. [9] have proposed such a robust version of the Capon beamformer that can still be solved in an efficient manner. Their approach has been adopted in this paper for robust Capon beamforming and in the following we indicate the steps to compute the robust Capon beamformer. The computation of the robust Capon beamformer consists of the following steps:

1. Determine the eigen-decomposition of the sample covariance matrix R

$$\mathbf{R} = \mathbf{U}\mathbf{D}\mathbf{U}^H \tag{3}$$

and set

$$\mathbf{b} = \mathbf{U}^H \bar{\mathbf{a}}. \tag{4}$$

2. Solve

$$\sum_{m=1}^{K} \frac{|b_m|^2}{(1+\lambda\gamma_m)^2} = \epsilon \tag{5}$$

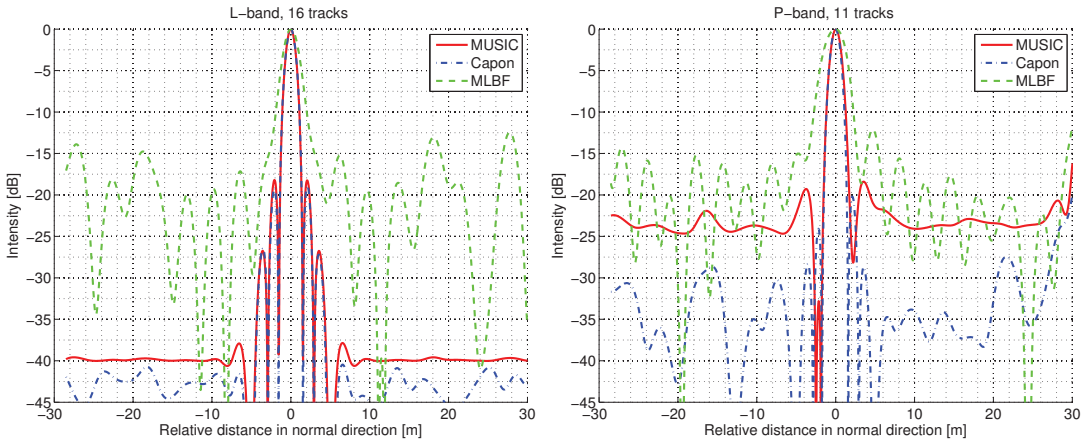

Fig. 3. Impulse Response obtained from an in-scene trihedral reflector

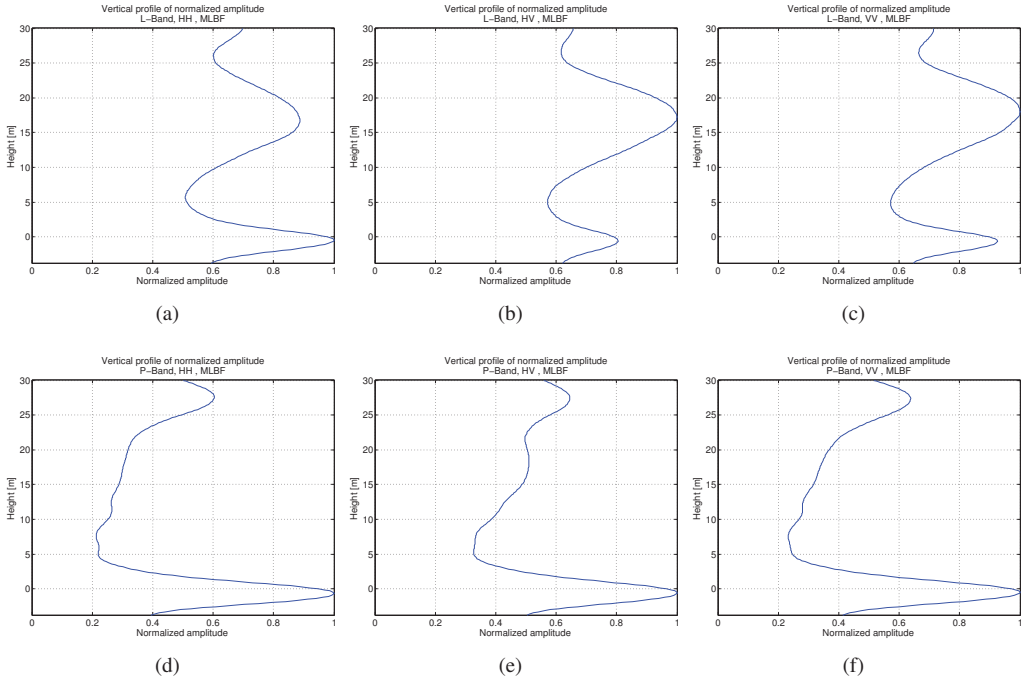

Fig. 4. Example of a vertical amplitude profile for multi-look standard beamforming at L-band and P-band for the polarimetric channels HH, VH, and VV. The ground level has been adjusted for each voxel according to an accurate digital elevation model obtained from airborne laser scanning. The local maxima that occur above 25 m above ground are due to the limited unambiguous height.

for the Lagrange multiplier λ, given the fact, that there is a unique solution in the interval $[\lambda_{low}, \lambda_{up}]$ [see [10]], where

$$\lambda_{low} = \frac{\|\bar{\mathbf{a}}\| - \sqrt{\epsilon}}{\gamma_1 \sqrt{\epsilon}}\ ,\ \lambda_{up} = \frac{\|\bar{\mathbf{a}}\| - \sqrt{\epsilon}}{\gamma_K \sqrt{\epsilon}} \tag{6}$$

3. Calculate an estimate of the unknown steering vector $\mathbf{a}$

$$\mathbf{a} = \bar{\mathbf{a}} - \mathbf{U}(\mathbf{I} + \lambda \mathbf{D})^{-1}\mathbf{b}. \tag{7}$$

4. The estimated power finally yields [10]

$$P_C = \frac{\|\mathbf{a}\|^2}{K\mathbf{a}^H\mathbf{R}^{-1}\mathbf{a}} = \frac{\mathbf{a}^H\mathbf{a}}{K\mathbf{a}^H\mathbf{U}\mathbf{D}^{-1}\mathbf{U}^H\mathbf{a}}. \tag{8}$$

3. DISCUSSION

We have successfully produced tomographic 3D images of a forested area (400 m x 900 m) obtained from airborne multi-

baseline SAR data at L- and P-band using three techniques, (1) multi-look beamforming, (2) robust Capon beamforming, and (3) MUSIC for the focusing in the normal direction. To the authors' knowledge, for the first time tomographic images of a single test site are now available at both, P- and L-band, obtained from two quasi-synchronous missions (time-span: 1 day). Excerpts of the 3D data sets and analyses thereof were presented in this paper. The performance of the focusing approaches has been demonstrated by means of the impulse responses obtained from an in-scene corner reflector. Both, MUSIC and robust Capon beamforming show their super-resolution properties and an improved side lobe reduction compared to the multi-look beamforming method. However, the true spectral power signal and the coherent character of the image are lost. Thus, MUSIC and robust Capon beamforming are the methods of choice rather for target detection purposes than for a further analysis of the back-scattering mechanisms.

The profiles of the normalized amplitudes show a striking difference in terms of the location of dominant back-scatterers for the two wavelengths: at L-band, back-scattering from the canopy is present for *all* polarizations, whereas, at P-band only the HV channel exhibits a (very moderate) local maximum at the canopy level.

However, in both cases, L- and P-band, the minimum in all profiles is found between canopy and ground surface, the minimum being more distinct in the L-band case, though.

Interestingly enough, at L-band not only the HH and the VV channel but also the HV channel shows a considerable back-scattering contribution at the ground level. In the P-band case, back-scattering occurs predominantly at the ground level for all channels.

The results and discussion part will be extended in the final paper.

4. REFERENCES

[1] A. Reigber and A. Moreira, "First demonstration of airborne SAR tomography using multibaseline L-band data," *IEEE Trans. Geosci. Remote Sens.*, vol. 38, no. 5, pp. 2142–2152, 2000.

[2] F. Lombardini and A. Reigber, "Adaptive spectral estimation for multibaseline SAR tomography with airborne L-band data," in *Proc. IEEE Int. Geosci. and Remote Sens. Symp.*, vol. 3, 2003, pp. 2014–2016.

[3] A. Reigber, M. Neumann, S. Guillaso, S. Sauer, and L. Ferro-Famil, "Evaluating PolInSAR parameter estimation using tomographic imaging results," in *Radar Conference, 2005. EURAD 2005. European*, 2005, pp. 189–192.

[4] O. Frey, F. Morsdorf, and E. Meier, "Tomographic imaging of a forested area by airborne multi-baseline P-band SAR," *Sensors, Special Issue on Synthetic Aperture Radar*, vol. 8, no. 9, pp. 5884–5896, Sept. 2008.

[5] O. Frey and E. Meier, "Combining time-domain back-projection and Capon beamforming for tomographic SAR processing," in *Proc. IEEE Int. Geosci. and Remote Sens. Symp.*, 2008, pp. 445–448.

[6] R. O. Schmidt, "Multiple emitter location and signal parameter estimation," *IEEE Trans. Antennas Propag.*, vol. 34, no. 3, pp. 276–280, Mar. 1986.

[7] P. Stoica, Z. Wang, and J. Li, "Extended derivations of MUSIC in the presence of steering vector errors," *IEEE Transactions on Signal Processing*, vol. 53, no. 3, pp. 1209–1211, Mar. 2005.

[8] J. Li, P. Stoica, and Z. Wang, "On robust Capon beamforming and diagonal loading," *IEEE Trans. Signal Process.*, vol. 51, no. 7, pp. 1702–1715, 2003.

[9] P. Stoica, Z. Wang, and J. Li, "Robust Capon beamforming," *IEEE Signal Processing Letters*, vol. 10, no. 6, pp. 172–175, June 2003.

[10] P. Stoica and R. L. Moses, *Spectral Analysis of Signals*. Upper Saddle River, NJ: Prentice Hall, 2005.